Macromolecules

Article

pubs.acs.org/Macromolecules

Progression of Alignment in Thin Films of Cylinder-Forming Block Copolymers upon Shearing

Raleigh L. Davis,[†] Brian T. Michal,[†] Paul M. Chaikin,[‡] and Richard A. Register*[,†]

[†]Department of Chemical and Biological Engineering and Princeton Institute for the Science and Technology of Materials, Princeton University, Princeton, New Jersey 08544, United States

[‡]Department of Physics, New York University, New York, New York 10003, United States

Supporting Information

ABSTRACT: Application of shear stress at the surface of a block copolymer thin film has been shown to substantially orient the microdomains in the direction of the applied shear. The present work systematically examines the influence of key material, film, and process parameters on this alignment behavior using a series of cylinder-forming polystyrene−poly(*n*-hexyl methacrylate) copolymers. A parallel plate rheometer applies a radially dependent stress gradient to the film's surface through a viscous nonsolvent overlayer. The degree of alignment is assessed using atomic force microscopy and examined as a function of the applied stress. To quantitatively compare the alignment process across different block copolymer films, a melting−recrystallization model is fit to the data, which allows for the determination of two key alignment parameters: the critical stress needed for alignment and an orientation rate constant. For films containing a monolayer of cylindrical domains, as polystyrene weight fraction or overall molecular weight increases, the critical stress increases moderately, while the rate of alignment drastically decreases. As the number of layers of cylinders in the film increases, the critical stress decreases modestly, while the rate remains unchanged. Substrate wetting condition has no measurable influence on alignment response over the range of conditions investigated. Collectively, these results provide useful quantitative rules that enable predictions of the level of alignment which will occur under particular shearing conditions.

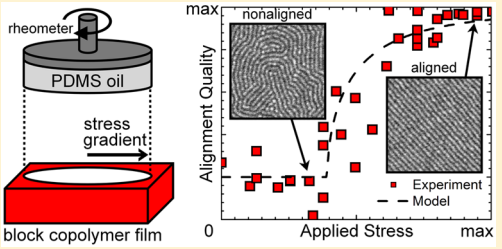

INTRODUCTION

Block copolymers have received much attention for their powerful ability to self-assemble into well-defined periodic nanostructures in the bulk.[1,2] More recently, thin films (∼10−100 nm) of these materials have garnered enormous interest for their potential use as patterning templates for various nanolithographic processes.[3−9] To be useful for these and related applications, however, there is a paramount need to develop strategies that can control the orientation of the microdomains. Numerous methods have been developed to this end,[9−17] including various zone annealing strategies,[18,19] the use of external fields,[20−22] and modifying the local or global substrate chemistry or topography.[23−28] One method that has been shown to impart strong in-plane alignment to block copolymer thin films is the application of shear stress at the film surface. Shear has long been known to orient block copolymer microdomains in the bulk,[29−33] but more recently, several methods have been developed to adapt this approach for thin films. Angelescu et al. achieved alignment in monolayers of a cylinder-forming block copolymer by placing a smooth, cross-linked poly(dimethylsiloxane) pad in contact with the film and applying a lateral force.[34] Given sufficient stress, the cylinders align in the shear direction over the entire area under the pad. This technique has been further shown to orient other cylinder-,[35−41] sphere-,[42] and lamellae-forming[43] block copolymers. Other groups have modified this technique by imparting shear via expansion of the elastomer pad upon heating[44,45] or swelling in solvent vapor.[46−49] Alternatively, a nonsolvent fluid can be used as the medium to impart stress at the film's surface. In one method the shear is applied by sandwiching a viscous silicone oil layer between the substrate-supported thin film and a rheometer plate. Rotation of the plate transmits a shear stress through the silicone oil to the film's surface.[50−53] A related shear alignment technique uses pressure-driven flow of the nonsolvent fluid (silicone oil) through a channel which directs the fluid across the film's surface.[54] The chief advantage of both of these techniques, as compared to the elastic pad shearing approach, is their ability to apply a range of stresses to a single sample, varying in position. This markedly increases the throughput and reliability of experiments intended to investigate how the quality of shear alignment varies with stress. These methods also avoid any "preshearing" caused by unintended or uncontrolled thermal expansion of the pad during specimen heating, between the block copolymer's upper glass transition temperature and the melt temperature to which the block copolymer is heated for shearing, prior to applying the shear stress.

Received: May 13, 2015
Revised: July 10, 2015
Published: July 24, 2015

DOI: 10.1021/acs.macromol.5b01028
Macromolecules 2015, 48, 5339−5347

While shear alignment has successfully produced well-ordered films, there is still much to be discovered regarding the factors which influence the ease and ultimate quality of alignment in shear-aligned films. Previous work has shown that the magnitude of the applied stress,[50−54] the time and temperature of shear,[50] and the polymer film thickness,[34,39] specifically its proximity to the preferred monolayer thickness, can all drastically influence the alignment quality. In addition, the mechanism by which alignment occurs is still an open topic. To model shear alignment in sphere-formers, Wu et al. proposed that any polymer grains that are misaligned relative to the direction of the applied shear experience an effective reduction in their order−disorder transition temperature; with sufficient stress, the most misaligned grains will selectively melt and reorder in the shear direction.[50] They described this phenomenon with a "melting−recrystallization model" and showed that this model reproduces the dependence of alignment quality on applied shear stress reasonably well for sphere-formers.[50,51] Later, Pelletier et al. modified this model for cylinder-formers and also found good agreement with experimental data.[54] To further test the core premise of this model, that the grains which are most misaligned with the shear direction are preferentially destroyed, Marencic et al. first aligned a polygrain film via shear and then systematically probed the effects of applied stress and misorientation angle on reorientation of the microdomains. They showed that the stress required for alignment increased monotonically as the difference between the microdomains' orientation and the shear direction decreased.[52]

The chief aim of the present work is to systematically examine the influence of key material, film, and process parameters on the alignment behavior (alignment quality vs stress and time) of cylinder-forming block copolymers. The parameters studied are the weight fraction of the cylinder-forming block, overall molecular weight, film thickness (number of cylinder layers), and wetting condition at the substrate. To examine these, we use a series of low-dispersity, cylinder-forming polystyrene−poly(*n*-hexyl methacrylate) block copolymers (PS−PHMA, PS minority block) and shear them using the rotational rheometer apparatus described above. Their alignment quality is assessed via atomic force microscopy and compared to the melting−recrystallization model, which provides a convenient method to systematically and quantitatively interpret the data.

EXPERIMENTAL SECTION

Materials. A series of PS−PHMA block copolymers of low dispersity ($Đ$), systematically varying in weight fraction of PS (w_{PS}) or overall number-average molecular weight (M_n), were synthesized via sequential living anionic polymerization of styrene (S) and *n*-hexyl methacrylate (HMA). All diblocks are referred to as PS−PHMA *X*−*Y*, where *X* and *Y* denote the PS and PHMA block M_n values, respectively. The detailed procedure for the synthesis of PS−PHMA 21−77 (previously denoted[55] as PS−PHMA 24−89) has been described by Nikoubashman et al.[55] PS−PHMA 31−108, 60−191, and 87−256 were synthesized by an identical procedure. PS−PHMA 30−86, 34−77, and 48−88 (previously denoted[39] PS−PHMA-26, -30, and -35, respectively) were synthesized using the same chemistry but in a different apparatus as described previously.[39] For all seven polymers, $Đ$ and M_n were determined via size-exclusion chromatography in tetrahydrofuran (THF) using a Waters 515 HPLC pump, two 30 cm Agilent PLgel Mixed-C columns operating at 35 °C, and Wyatt OptiLab T-rEX (differential refractive index, DRI) and miniDAWN TREOS (three-angle light scattering) detectors, both operating at 658 nm and 25 °C. The specific refractive index increments, d*n*/d*c*, of PS (0.1834 mL/g) and PHMA (0.0752 mL/g) homopolymers in THF were measured at these conditions using a separate Wyatt OptiLab rEX. The molar compositions of the block copolymers, and thereby w_{PS}, were measured using ^{1}H NMR spectroscopy in $CDCl_3$ on a Bruker AVANCE by comparing the peak areas of the PS aromatic protons (6.3−7.2 ppm) and the PHMA methylene protons (3.7−4.2 ppm). The reported diblock M_n values were computed using the absolute weight-average molecular weights (M_w) obtained from the light scattering data, using a weight-fraction-weighted d*n*/d*c*,[56] and the $Đ$ measured from the DRI data. The PS block M_n is calculated by taking the product of the diblock M_n and w_{PS}, while $Đ$ is obtained from the DRI data acquired from a PS block aliquot taken during the polymerization. The bulk morphology was measured using one-dimensional small-angle X-ray scattering (SAXS), using Cu Kα radiation from a PANalytical PW3030 generator with long-fine-focus Cu tube, a slit-collimated Anton Paar compact Kratky camera, an MBraun OED-50 M position sensitive detector, and a home-built hotstage.[57] Data were corrected for empty beam scattering, sample thickness, and transmittance, compared to a polyethylene standard for absolute intensity, and desmeared.[57] The spacing between layers of cylinders in bulk (d_{bulk}) was measured at 150 °C via $d_{bulk} = 2\pi/q^*$, where q^* is the primary SAXS peak position. Table 1 displays the characteristics of the seven PS−PHMAs used in this study.

Table 1. Summary of Characteristics of PS−PHMA Diblock Copolymers

PS−PHMA	w_{PS}	PS M_n [kg/mol]	PS $Đ$	diblock M_n [kg/mol]	diblock $Đ$	d_{bulk} [nm]
21−77	0.21	20.7	1.05	98	1.10	32.2
30−86	0.26	29.7	1.15	116	1.08	38.3
34−77	0.30	33.5	1.13	111	1.06	39.8
48−88	0.35	47.9	1.10	136	1.09	47.0
31−108	0.22	30.7	1.13	139	1.10	39.6
60−191	0.24	60.3	1.13	251	1.16	57.2
87−256	0.25	87.3	1.08	344	1.05	85.4

Thin Film Preparation and Shear Alignment. Solutions of PS−PHMA in toluene (~1−5 wt %) were prepared and spin-cast onto silicon wafers (SiliconQuest, with native oxide), producing thin films of uniform thickness, *t* (±1 nm). The wafers were liberally rinsed with toluene (ACS reagent grade, Fisher Scientific) prior to use. After deposition, the films were thermally annealed under vacuum for 2 h at 150 °C, well above the glass transition temperature, T_g, for both blocks (for PS homopolymer,[58] T_g = 100 °C, while for PHMA homopolymer, T_g = 8 °C; see Figure S1 in Supporting Information). Film thicknesses, prior to and after annealing, were measured using a Gaertner Scientific LS116S300 ellipsometer (wavelength = 632.8 nm) and consistently agreed within ±0.5 nm, indicating that insignificant residual solvent was present in the as-spun films.

The PS−PHMA films were shear-aligned as follows. The supported films were fastened with polyimide tape directly to a Peltier heating plate, which is attached to an Anton Paar MCR-501 rheometer fitted with a 25 mm diameter parallel plate.[50,51] Highly viscous poly(dimethylsiloxane) (PDMS) oil (DMS-T72, purchased from Gelest, room temperature kinematic viscosity ≈2 × 10^7 cSt) is placed on the surface of the film, after which the parallel plate is carefully lowered until the PDMS layer between the plate and block copolymer film is ~0.2 mm (the oil is trimmed around the plate's edge when the gap height is ~0.21−0.22 mm). A schematic of this setup is shown in Figure 1a. Once the oil no longer exerts a measurable upward normal force on the plate, indicating that any stresses in the oil have relaxed, the Peltier plate is heated to 150 °C and allowed to equilibrate for 15 min. The shear is then applied by rotating the top plate with a constant torque, thus creating a radially varying shear stress gradient such that the stress at the film's center is zero and increases to a maximum at the plate's edge (this gradient is shown in Figure 1b). After shearing for a prescribed time (t_{shear}), the system is cooled to room temperature (at a rate of ~25 °C/min for t_{shear} > 30 min and ~100 °C/min for t_{shear} < 30

DOI: 10.1021/acs.macromol.5b01028
Macromolecules 2015, 48, 5339−5347

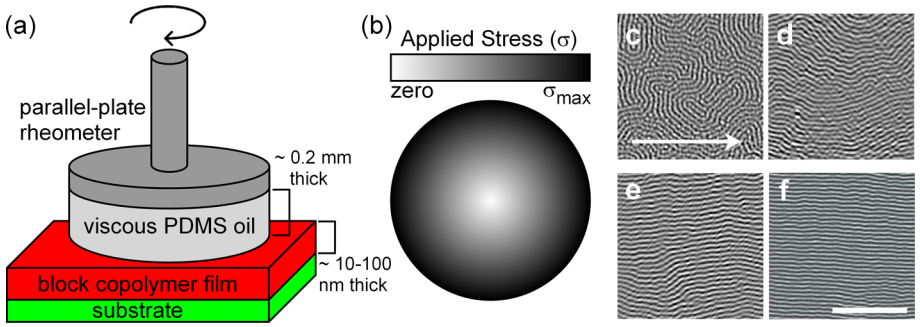

Figure 1. (a) Schematic of the experimental setup for imparting a gradient of shear stress to a polymer film using a parallel plate rheometer. (b) Top-down view of the applied stress gradient. (c–f) Representative AFM phase images from a monolayer of PS–PHMA 21–77, sheared at 150 °C for 30 min, showing the progressive increase in alignment quality as the applied stress is increased: (c) 0 Pa (order parameter ψ_2 = 0.09, computed over the entire 2 μm × 2 μm area of the full image), (d) 800 Pa (ψ_2 = 0.51), (e) 1200 Pa (ψ_2 = 0.82), and (f) 2000 Pa (ψ_2 = 0.98). Scale bar = 500 nm.

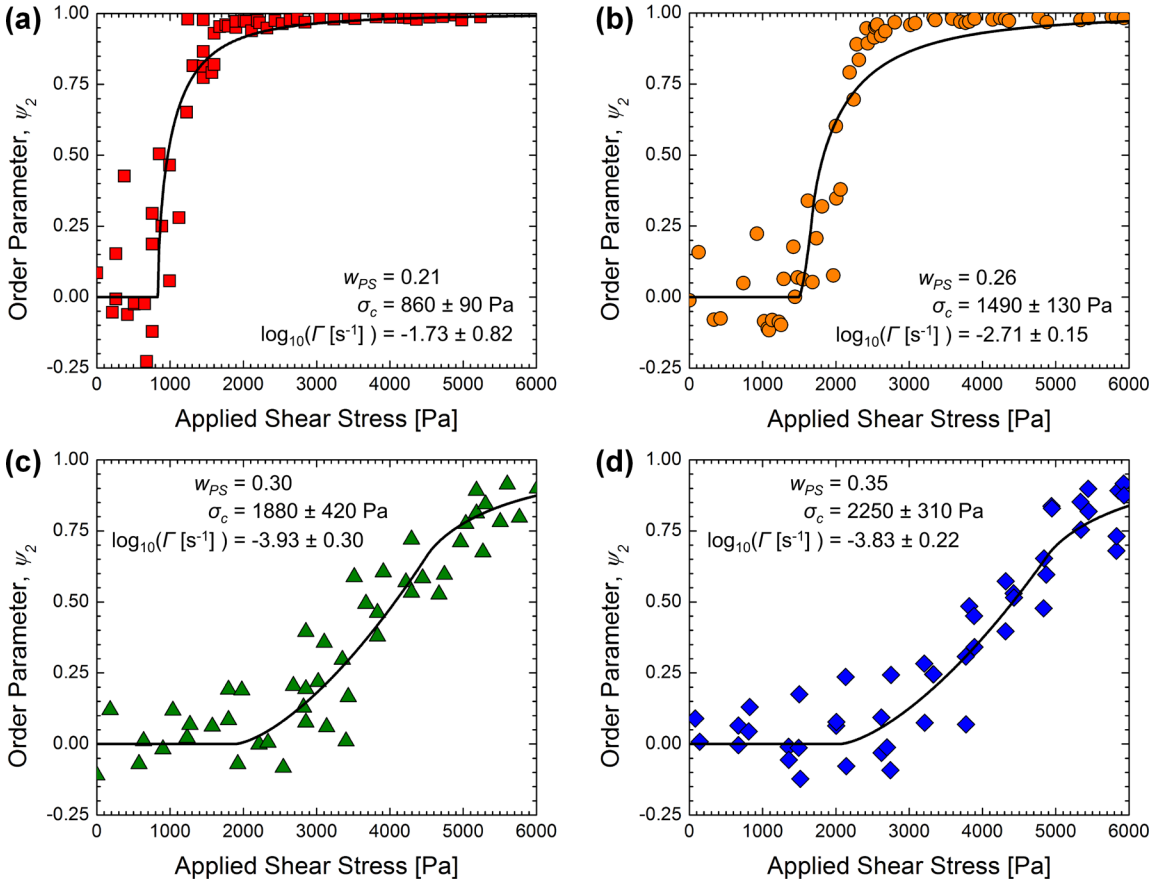

Figure 2. Alignment quality, measured by ψ_2, as a function of applied shear stress for (a) PS–PHMA 21–77, (b) 30–86, (c) 34–77, and (d) 48–88, all after 30 min of shearing at 150 °C. Symbols correspond to experimental values determined from TM-AFM phase images of the sheared films, while the black lines show the least-squares fits of the melting–recrystallization model to the experiments. The best-fit model parameter values for each polymer are displayed in the corresponding graphs, with ±1 standard deviation of the fit.

min) with the stress still applied. This ensures that any shear-induced alignment is "locked in" as the system is cooled below the T_g of the PS cylinders. After completion of the process, a circular outline around the shearing plate is scribed into the wafer to later identify the center of the sheared area. Once the plate is raised, the excess PDMS oil on the film surface is removed by "sponging" it off using a cross-linked PDMS pad; the PDMS oil preferentially wets the pad and detaches from the block copolymer film surface. The pad is prepared by casting a mixture of Dow Corning Sylgard 184, at a weight ratio of 1:15 curing agent to elastomer, onto a Si wafer and curing at ∼60 °C for 2 h and then overnight at room temperature.

Imaging and Data Analysis. PS–PHMA thin film morphology was characterized at room temperature using atomic force microscopy (AFM, Digital Instruments Dimension 3000) operated in tapping mode (TM) using force modulation mode probes (NanoWorld, force constant = 1.2–5.5 N/m, resonance frequency = 60–90 kHz). Despite AFM being a surface characterization technique, the large mechanical contrast between the glassy PS cylinders and rubbery PHMA matrix enables investigation of the underlying cylinders via phase contrast imaging. All images were taken at 512 × 512 pixel resolution with a scan size of 2 μm × 2 μm.

DOI: 10.1021/acs.macromol.5b01028
Macromolecules 2015, 48, 5339–5347

The degree of alignment of the cylinders in the direction of applied shear in a particular micrograph can be quantified using an orientational order parameter $\psi_{2\alpha}$, defined as follows:

$$\psi_{2\alpha} = \langle \cos[2\alpha(\theta_i - \theta_0)] \rangle \quad (1)$$

where θ_i is the direction of microdomain orientation, θ_0 is the direction of applied shear, and $\alpha = 1$ for systems with a 2-fold symmetric lattice, while $\alpha = 3$ is used for 6-fold symmetric patterns. The order parameter is equal to 0 when the microdomains are randomly oriented, 1 when they are perfectly aligned, and −1 when antialigned. In the present work, ψ_2 is predominantly employed; however, in some cases where both in- and out-of-plane cylinders are present,[39] ψ_6 is used instead. Because of the factor of α in their definitions, the numerical value of $(1 - \psi_6)$ for a well-aligned film is 9 times the value of $(1 - \psi_2)$;[53] for example, an aligned image with $\psi_2 \approx 0.99$ would have $\psi_6 \approx 0.90$. Details for how ψ_2 and ψ_6 are computed are discussed elsewhere.[39,52,53] Prior to calculating the order parameter, the micrographs are filtered by performing a discrete Fourier transform, removing high- and low-frequency noise, and transforming back to real space. Images which are poorly aligned, or which contain dots, are filtered using an annular mask in reciprocal space, while highly aligned images are filtered more aggressively using a mask consisting of two circles centered around the two first-order peaks in Fourier space.

The applied shear stress, σ, at a given position on the film can be determined as a function of the radial distance from the center of the sheared area, r, by first computing the shear rate, $\dot{\gamma}$, via

$$\dot{\gamma}(r) = r\Omega/H \quad (2)$$

where Ω is the angular velocity [rad/s] of the rheometer plate and H is the distance between the plate and the polymer film.[59] The local viscosity of the PDMS layer, η, can be computed using the Carreau−Yasuda constitutive equation:[60]

$$\eta(r) = \eta_0[1 + (\lambda\dot{\gamma}(r))^a]^{(n-1)/a} \quad (3)$$

where the fitting parameters η_0 (the zero shear viscosity), λ, a, and n were determined by measuring the PDMS oil viscosity as a function of shear rate (from 0.02 to 2 s^{-1}, the range over which shear alignment was conducted) using a cone-and-plate tool and fitting to eq 3 (see Figure S2 in the Supporting Information). The local shear stress is then computed by

$$\sigma(r) = \eta(r) \times \dot{\gamma}(r) \quad (4)$$

To calculate r for a particular image, the center of the sheared area was determined as described previously,[52] and r was then computed from the position of the AFM image.

RESULTS AND ANALYSIS

Influence of Polymer Composition. Monolayers of PS−PHMA 21−77 (t = 28 nm), 30−86 (t = 39 nm), 34−77 (t = 39 nm), and 48−88 (t = 47 nm)[39] were sheared using stresses ranging from 0 to 6000 Pa. These four polymers systematically vary in w_{PS} but have nearly constant overall M_n. Examination of the sheared samples by AFM revealed the dependence of alignment quality on applied shear stress as displayed in Figure 2. At the lowest stresses, before any significant alignment occurs, ψ_2 scatters randomly around a value of zero; the sizable magnitude of the scatter reflects the fact that the average grain size is not vastly smaller than the AFM image size. Above a threshold stress, which monotonically increases with w_{PS}, the cylinders begin to align, leading to an increase in ψ_2 until it reaches a plateau value. For the two lowest-w_{PS} polymers, PS−PHMA 21−77 and 30−86, the transition from nonaligned to well-aligned occurs over a narrow range of applied stresses (~1000 Pa wide), while the two higher-w_{PS} polymers, PS−PHMA 34−77 and 48−88, display much broader transition ranges (>4000 Pa wide) and appear not to have reached their terminal alignment quality at the maximum stress applied. The upper limit of applied stress accessible in this particular setup was limited by the tendency of the oil to escape the gap over time, the result of outward normal forces exerted by the oil due to its viscoelasticity.[59] For shear times of ~0.5−2 h, 6 kPa is the largest maximum stress which can be imparted before any leaking becomes detectable.

To quantitatively compare the four block copolymers and to gain further insight into the origin of the differences in alignment behavior as a function of composition, these data were compared to the melting−recrystallization model, first described for cylinder-formers by Pelletier et al.[54] The model states that cylinders which are sheared at an angle to their axis experience an effective reduction in their order−disorder transition temperature, T_{ODT}, the strength of which depends on the magnitude of the applied stress and the degree of misalignment to the shear direction, as shown in eq 5:

$$T^*_{ODT} = T_{ODT}\left(1 - \left(\frac{\sigma}{\sigma_c}\right)^2 \sin^2(\alpha(\theta - \theta_0))\right) \quad (5)$$

where T^*_{ODT} is the effective T_{ODT}, σ is the applied shear stress, $\theta - \theta_0$ is the misorientation of a grain with respect to the shear direction, and σ_c is a parameter termed the critical stress. Equation 5 is derived from a Landau model[61,62] with an added anisotropic diffusion term which represents the energy induced by shearing. Using phenomenological and symmetry arguments proposed by Angelescu et al.,[34] this diffusion term is set as proportional to the shear rate squared; this is the origin of the exponent of 2 on the stress and sine terms in eq 5 (note that in the model derived for sphere-formers, the stress has an exponent of unity[50]).

When T^*_{ODT} is less than the shearing temperature, T, the misoriented grains "melt" and then recrystallize in the direction of applied shear. The rates of melting and recrystallization, which are assumed equal, are given by

$$\frac{\partial R(\theta - \theta_0)}{\partial t} = \Gamma\frac{(T^*_{ODT} - T)}{T_{ODT}} \quad (6)$$

where R is the area of a grain and Γ is a rate constant which describes how quickly the limiting alignment is reached. The predicted degree of alignment can then be computed by

$$\psi_{2\alpha} = D\frac{\int_0^{\pi/\alpha} R(\theta - \theta_0)\cos(2\alpha(\theta - \theta_0))\,\mathrm{d}(\theta - \theta_0)}{\int_0^{\pi/\alpha} R(\theta - \theta_0)\,\mathrm{d}(\theta - \theta_0)} \quad (7)$$

where D is a Debye−Waller-like term which reflects the terminal quality of order at high stresses. In the context of this study, the primary utility of the melting−recrystallization model is that the critical stress, σ_c, and alignment rate constant, Γ, can be extracted via a best fit of the model to each data set, providing a convenient, quantitative comparison across experiments.

The melting−recrystallization model was fit to the four data sets (shown as solid lines in Figure 2). Since the polymers all appear to approach $\psi_2 = 1$ at high stress, we set $D = 1$. In addition, because none of the polymers studied possess a thermally accessible T_{ODT} (the materials degrade before T_{ODT} can be reached), we estimated the T_{ODT} for each diblock using the available literature (see the Supporting Information for

DOI: 10.1021/acs.macromol.5b01028
Macromolecules 2015, 48, 5339−5347

details; estimated values of the segregation strength χN at 150 °C range from 28 to 98 across the series); because the Flory–Huggins interaction parameter for PS–PHMA is known to be very weakly dependent on temperature,[63,64] all the estimated T_{ODT} values are quite high (>400 °C), in the regime where the model prediction is insensitive to the value of T_{ODT} ($T_{ODT} \gg T$). The best-fit parameters for the four polymers as functions of w_{PS} are shown in Figure 3. Standard deviations for the best-fit model parameters were generated via a bootstrapping algorithm (see Supporting Information for details).[65] Also shown in Figure 3 are the best-fit values of σ_c and Γ for a monolayer (t = 35 nm) of a 50:50 blend (by weight) of PS–PHMA 30–86 (w_{PS} = 0.26) and 34–77 (w_{PS} = 0.30), which has w_{PS} = 0.28 (for ψ_2 vs stress for this blend, see Figure S8 in the Supporting Information). In general, the ψ_2 vs applied stress behavior is well matched by the model, though the data for PS–PHMA 30–86 (Figure 2b) show a steeper transition from nonaligned to aligned than the model captures.

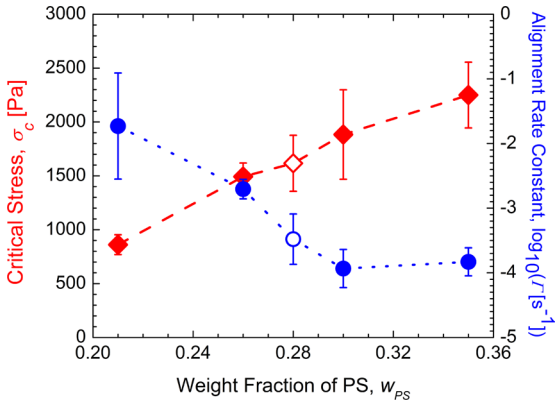

Figure 3. Values of the critical stress, σ_c (red diamonds), and alignment rate constant, Γ (blue circles), from the melting–recrystallization model fits in Figure 2, plotted against the weight fraction of minority block in the copolymer. Filled symbols indicate neat block copolymers, while the open symbols show the results from a copolymer blend. Error bars indicate ±1 standard deviation of the model fit.

As w_{PS} increases, σ_c increases nearly linearly, while over the same range, Γ decreases by more than an order of magnitude. The model thus indicates that any apparent qualitative difference between the polymers with sharp and gradual alignment transitions may be understood through their substantial, but smoothly varying, differences in alignment rates. To explore this idea further, additional experiments were done with the "fastest" (21–77) and "slowest" (48–88) polymers in this set, in which identical monolayer films were sheared under the same conditions but for shear durations varying over the practical range. The minimum shear time is dictated by the maximum cooling speed of the Peltier plate (~100 °C/min); a minimum shear time of 5 min was chosen, to reduce the influence of the ~0.5 min cool (under shear) from 150 °C to the PS T_g. Conversely, the maximum shear time is limited by the oil leakage from the gap described earlier, ~2 h for the stresses of interest. Using the best-fit σ_c and Γ previously measured for each polymer, we compute the ψ_2 vs σ behavior expected for various shear times and compare with the analogous experiments (Figure 4). The model prediction for the "fast" polymer shows that Γ is sufficiently large that even 5 min of shear produces the limiting quality of alignment at each stress; this prediction is well corroborated by the experiments. In the case of the "slow" polymer, the model shows a substantial time dependence over the range investigated that is in remarkable agreement with the data (within the experimental scatter). These results provide compelling evidence that the melting–recrystallization model accurately captures the kinetics of the shear alignment process.

Molecular Weight Scaling. The above results illustrate that for nearly constant overall molecular weight σ_c increases and Γ decreases monotonically with increasing w_{PS} across the cylinder-forming region. The following presents a complementary study in which composition was kept (nearly) constant, but molecular weight was varied by a factor of ~3.5. Monolayers of PS–PHMA 31–108 (t = 40 nm), 60–191 (t = 59 nm), and 87–256 (t = 86 nm; for determination of monolayer film thicknesses for these polymers, see Supporting Information) were sheared. At low stresses, before any substantial alignment occurs, the PS–PHMA 60–191 and 87–256 films displayed mixed patterns of both in-plane cylinders and hexagonally packed dots; these dots are likely cylinders which have reoriented perpendicular to the substrate.[39] While these mixed morphology patterns are consistent with those seen previously for PS–PHMA diblocks

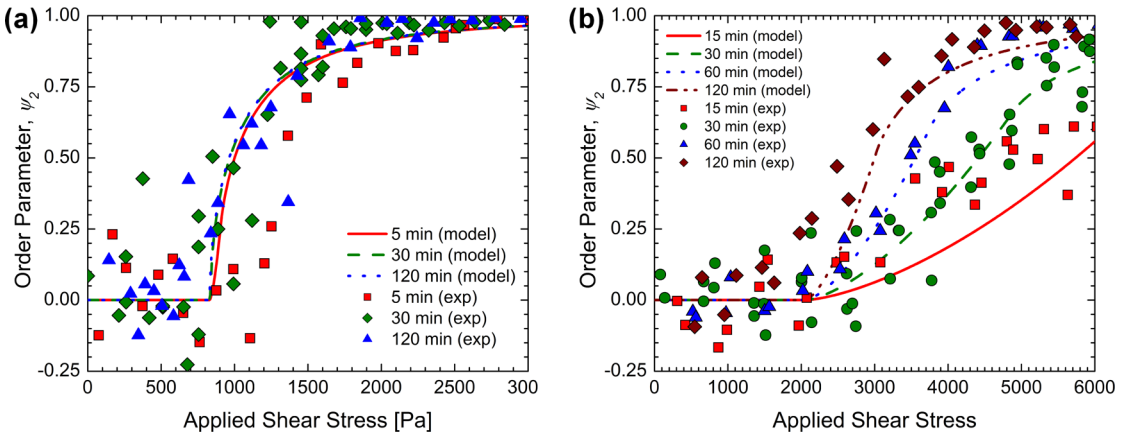

Figure 4. Alignment vs stress for (a) PS–PHMA 21–77 and (b) 48–88 for varying shear times. The symbols display the experimental results from TM-AFM, while the lines show the predictions of the melting–recrystallization model for each polymer: (a) PS–PHMA 21–77: σ_c = 860 Pa, $\log(\Gamma\ [s^{-1}])$ = −1.73; (b) PS–PHMA 48–88: σ_c = 2250 Pa, $\log(\Gamma\ [s^{-1}])$ = −3.83.

DOI: 10.1021/acs.macromol.5b01028
Macromolecules 2015, 48, 5339–5347

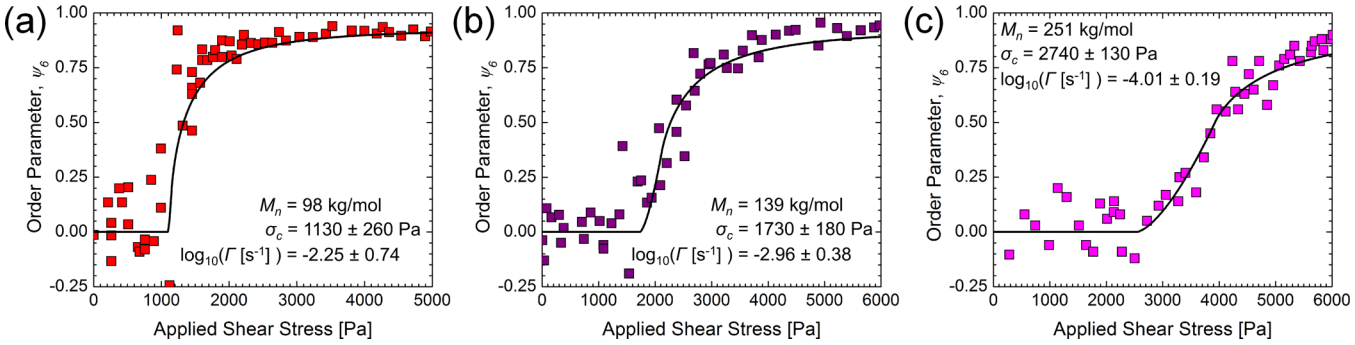

Figure 5. Alignment quality, measured by ψ_6, vs applied shear stress for (a) PS−PHMA 21−77 sheared for 30 min (same sheared film for which data were presented in Figure 2a, but here using ψ_6, rather than ψ_2, to quantify the orientation), (b) 31−108 sheared for 30 min, and (c) 60−191 sheared for 2 h. The symbols show the experimental results, while lines show the best fits to the melting−recrystallization model.

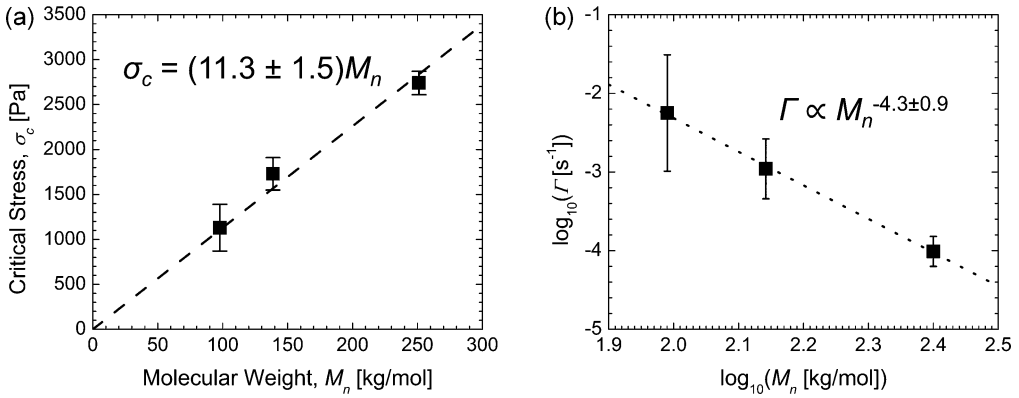

Figure 6. Best-fit parameter values from Figure 5 plotted vs molecular weight: (a) σ_c vs M_n; (b) log(Γ) vs log(M_n). Lines indicate the best fits to the data; error bars indicate ±1 standard deviation in the melting−recrystallization model fits.

at nonmonolayer thicknesses,[39] it is unusual that these patterns persist even in monolayer films of the present polymers. To accurately capture any alignment of these dots, we employ ψ_6 here in place of ψ_2, even in instances in which the polymer shows no dots (PS−PHMA 21−77 and 31−108). The experimental results and best fits to the melting−recrystallization model are displayed in Figure 5. PS−PHMA 87−256 showed no discernible alignment over the range of stresses employed and thus could not be meaningfully fit to the model (see Figure S10 in the Supporting Information). For these films, a terminal value of ψ_6 = 0.93 is observed in the data of Figure 5a, thus setting the value of D in eq 7 for these experiments.

The dependence of σ_c and Γ on molecular weight is shown in Figure 6. The critical stress scales linearly with M_n, while Γ shows a much stronger dependence, roughly scaling as $M_n^{-4.3\pm0.9}$. Previously, Γ was postulated to be proportional to the block copolymer's self-diffusion coefficient.[34] From classic reptation theory,[66−68] $D_S \propto M^{-2}$, but the scaling observed here for Γ with M_n is stronger. Indeed, Lodge and Dalvi,[69] and later Yokoyama and Kramer,[70,71] argued that self-diffusion should scale much more strongly with molecular weight for microphase-separated block copolymers because of a thermal activation barrier which must be overcome for chains to "hop" between microdomains. While a quantitative molecular interpretation of Γ remains elusive, the relationship displayed in Figure 6b is still useful to predict which PS−PHMA diblocks will or will not align under a particular set of shearing conditions. As an example, one can predict the quality of alignment expected for PS−PHMA 87−256 (the polymer which showed no alignment upon shearing) at the shear conditions employed (σ_{max} = 6000 Pa, t_{shear} = 120 min). Extrapolating to the appropriate molecular weight, the scaling relationships predict that PS−PHMA 87−256 should possess σ_c = 3890 Pa and $\Gamma = 2.5 \times 10^{-5}$ s^{-1}. Using these parameters, a model prediction was generated (see Figure S10 in Supporting Information), which showed that indeed no detectable alignment should occur. This fully corroborates our null observation and suggests that a shearing time of ∼10 h at 6 kPa (well above what we can achieve experimentally) would be needed to unambiguously observe alignment in this system.

Film Thickness, Wetting Condition, and Film−Substrate Interactions. In addition to molecular parameters such as w_{PS} and M_n, details concerning the film itself, specifically its thickness, wetting condition (whether the majority or minority block wets the substrate), and film−substrate interactions, can potentially influence the microdomains' response to shear. Previous work has shown that small deviations in film thickness away from the monolayer thickness can lead to substantial reductions in the quality of alignment observed upon shearing.[34,39] This effect was also observed in the present study; when sheared, PS−PHMA films with an incommensurate thickness require greater stresses before alignment occurs, and the terminal alignment quality is poor as compared to the monolayer case. At commensurate thicknesses (integer multiples of the monolayer thickness), the alignment behavior is qualitatively similar to the monolayer case.[39] As a complement to that work, the following experiments illustrate how the ease of alignment is influenced by film thickness/number of cylinder layers.

DOI: 10.1021/acs.macromol.5b01028
Macromolecules 2015, 48, 5339−5347

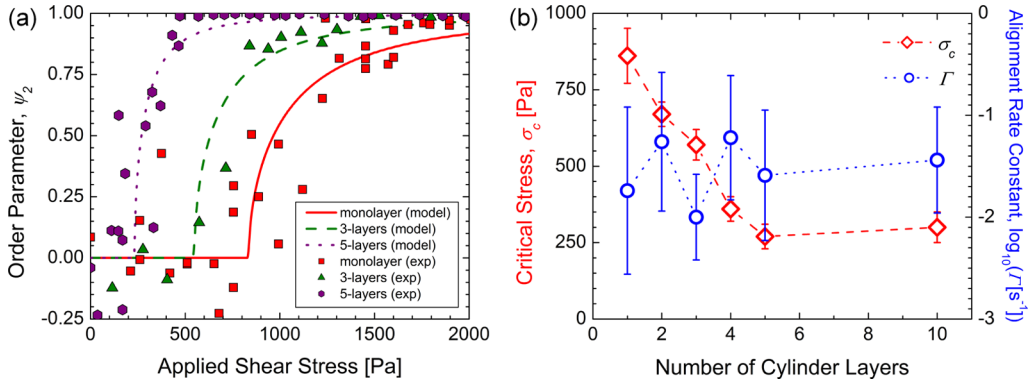

Figure 7. (a) Alignment (ψ_2) vs applied stress for PS−PHMA 21−77 films with thicknesses corresponding to 1 (red squares), 3 (green triangles), and 5 (purple hexagons) cylinder layers. Curves show the respective best fits to the melting−recrystallization model. Analogous data sets for 2, 4, and 10 layer thick films are shown in Figure S11 of the Supporting Information. (b) Best-fit parameter values vs number of cylinder layers: σ_c (red diamonds) and Γ (blue circles). Error bars indicate ±1 standard deviation in the model fits.

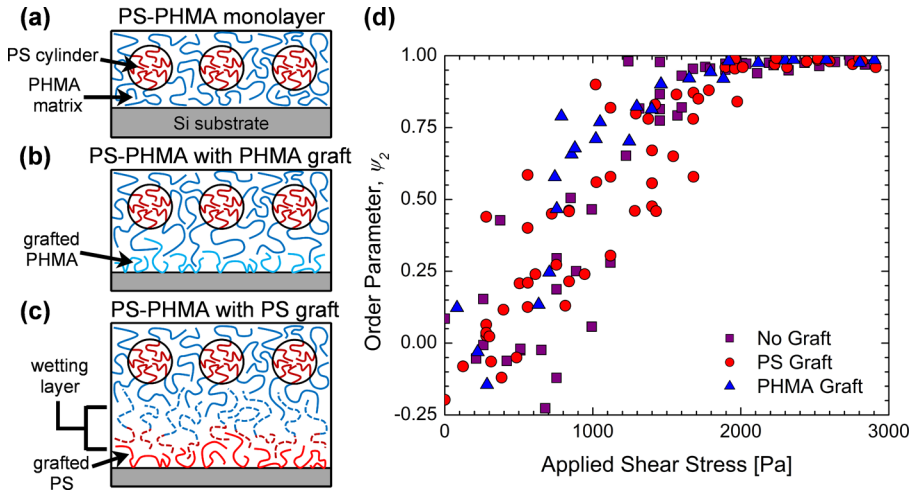

Figure 8. (a−c) Schematics of cylinder-forming PS−PHMA films on various substrates, with the PS blocks in red and the PHMA blocks in blue: (a) on Si substrate (gray) bearing the native oxide, (b) on a substrate grafted with PHMA chains (bright blue), and (c) on a substrate grafted with PS chains (bright red), where the brush-like wetting layer of block copolymer is indicated by the dashed chains. (d) Alignment (ψ_2) vs applied stress for monolayers of PS−PHMA 21−77 on bare Si wafer with native oxide (purple), on a layer of grafted PS (red), and on a layer of grafted PHMA (blue).

Films of PS−PHMA 21−77 corresponding to 2 (t = 57 nm), 3 (t = 85 nm), 4 (t = 115 nm), 5 (t = 143 nm), and 10 layers (t = 285 nm) of cylinders were sheared at T = 150 °C, t = 30 min, and $\sigma \approx$ 0−3000 Pa and compared with the results for the corresponding monolayer film. Selected results are displayed in Figure 7a (for the complete set of data, see Figure S11 in the Supporting Information). In all cases the same qualitative behavior is observed, with no alignment at the lowest stresses and a sharp transition to a well-aligned state at moderate stresses. Fitting the melting−recrystallization model to these data reveals the dependence of the alignment parameters on the number of cylinder layers (Figure 7b). The critical stress first decreases, by approximately 3×, perhaps reflecting a cooperativity between layers (with a hexagonal packing of cylinders), and then appears to plateau at about 4−5 layers. By contrast, the alignment rate constant shows no discernible trend within the scatter, consistent with the idea that Γ reflects an intrinsic material property (such as diffusivity) and would thus be unaffected by film thickness.

The substrate wetting condition of the film, and the "penetrability" of the substrate, were also examined for their effects on the alignment response. Monolayer films of PS−PHMA 21−77 were deposited on PHMA-preferential and PS-preferential substrates formed by grafting PHMA or PS layers onto Si wafers, as shown schematically in Figure 8 (see Supporting Information for details). The PHMA-grafted substrate (Figure 8b) yields the same wetting conditions for PS−PHMA as on the bare Si wafer (Figure 8a), for which alignment data were already shown in Figure 2a: the PHMA matrix wets both substrate and air interfaces. However, on the PHMA-grafted substrate, the PHMA blocks of the copolymer matrix could penetrate the substrate (the grafted layer) to some extent, while the bare Si wafer presents an impenetrable substrate. By contrast, the substrate wetting condition differs for the PS-grafted substrate (Figure 8c); in this case, an additional brush-like wetting layer of block copolymer,[72] having a thickness of approximately half a microdomain layer spacing, forms at the substrate so that the PS-grafted substrate is wetted by PS blocks (see Supporting Information). The cylindrical microdomains, and the chains that form them, "ride upon" this brush-like layer and thus do not contact the substrate.[73] The monolayer films were sheared at 150 °C for 30 min over a stress range of 0−5000 Pa; recall from Figure 2a that PS−PHMA 21−77 has "fast" alignment kinetics and thus should be well-aligned under these shear conditions. As shown in Figure 8d, no significant difference in alignment vs stress behavior was

DOI: 10.1021/acs.macromol.5b01028
Macromolecules 2015, 48, 5339−5347

observed among the three cases. Given the "fast" alignment of this polymer, it is perhaps unsurprising that no differences in alignment kinetics are observed; it would take a substantial change in Γ, half an order of magnitude or more, for this effect to be unambiguously detectable. However, the lack of change in σ_c, which can be measured in "fast" polymers with much more sensitivity, between the bare Si and PHMA-grafted substrates indicates that any penetration of the grafted layer by the block copolymer chains does not affect the stress required for microdomain alignment. Moreover, "decoupling" the chains which form the microdomains from the substrate, by creating the wetting layer in between via the PS-grafted substrate, does not affect the stress required for alignment. These results suggest that one can broadly change the surface energy (and therefore the substrate-wetting block), as well as the "penetrability" of the substrate surface, without compromising the alignment behavior of the overlying block copolymer layer.

CONCLUSIONS

In cylinder-forming PS−PHMA thin films, the cylinders retain their initial polygrain structure at low applied shear stresses, but with increased stress the cylinders transition from a nonaligned to a highly aligned state. The stress at which this transition occurs, as well as its breadth, is strongly dependent on the macromolecular characteristics of the block copolymer studied. All of the experiments were compared to a melting−recrystallization model through which two alignment parameters, a critical stress and an alignment rate constant, are extracted to provide a quantitative means of comparing across experiments. The critical stress needed to induce alignment increases linearly with PS weight fraction and overall block copolymer molecular weight; conversely, the rate of alignment dramatically decreases, with an especially strong dependence on molecular weight ($\Gamma \propto M_n^{-4.3\pm0.9}$). To confirm that the dramatic differences in the breadth of the nonaligned-to-aligned transition between different polymers were due to their substantial differences in Γ, select films were sheared identically, but for varying shear durations; the time dependence of the shear response was well reproduced by the model. Combining the model equations with the measured scaling rules for the model parameters thus provides an avenue for predicting alignment response for a given material under a specified set of shear conditions. In addition to the material properties discussed above, the effects of film properties (film thickness/number of cylinder layers, substrate wetting condition) were also assessed. The critical stress needed to induce alignment decreases with an increasing number of cylinder layers and reaches a plateau value at ∼5 layers thick. Interestingly, the alignment kinetics, which are highly sensitive to block copolymer composition and molecular weight, show no measurable dependence on film thickness. In addition, neither the block copolymer wetting condition nor the penetrability of the substrate surface was found to have a measurable impact on either σ_c or Γ. Moving forward, it would be interesting to see how the scaling trends observed here could suggest modifications of the shearing process to permit very rapid shear alignment of thin films of properly designed polymers. In addition, similar studies using other common block copolymer morphologies which are of interest to the nanolithography community (notably sphere- and lamellae-forming systems) might provide additional insight into the mechanisms underpinning shear alignment in block copolymer thin films.

ASSOCIATED CONTENT

Supporting Information

Dynamic mechanical thermal analysis data for a PHMA homopolymer; viscosity vs shear rate data for DMS-T72 PDMS oil and best fit to the Carreau−Yasuda model; T_{ODT} values used in the model fits and their estimation; details of the bootstrap analysis used to generate the uncertainty of the best fits of the melting−recrystallization model; optimal film thickness determination and shear alignment for the 50:50 blend of PS−PHMA 30−86 and 34−77; alignment vs film thickness data for PS−PHMA 31−108, 60−191, and 87−256; alignment vs stress data for PS−PHMA 87−256; a plot showing the complete data set used to generate the fit parameters shown in Figure 7b; details on the synthesis of the random copolymers used for substrate modification. The Supporting Information is available free of charge on the ACS Publications website at DOI: 10.1021/acs.macromol.5b01028.

AUTHOR INFORMATION

Corresponding Author

*Tel +1 609 258 4691; fax +1 609 258 0211; e-mail register@princeton.edu (R.A.R.).

Present Address

B.T.M.: Department of Macromolecular Science and Engineering, Case Western Reserve University, Cleveland, OH 44106.

Notes

The authors declare no competing financial interest.

ACKNOWLEDGMENTS

The authors gratefully acknowledge Carmeline Dsilva and Arash Nikoubashman for helpful discussions and Bryan Beckingham for some of the SAXS results included in Table 1. This work was generously supported by the National Science Foundation, MRSEC program, through the Princeton Center for Complex Materials (DMR-0819860 and DMR-1420541). P.M.C. gratefully acknowledges support from the National Science Foundation (DMR-1105417).

REFERENCES

(1) Bates, F. S. *Science* **1991**, *251*, 898−905.
(2) Hamley, I. W. *The Physics of Block Copolymers*; Oxford University Press: Oxford, 1998.
(3) Black, C. T.; Ruiz, R.; Breyta, G.; Cheng, J. Y.; Colburn, M. E.; Guarini, K. W.; Kim, H.-C.; Zhang, Y. *IBM J. Res. & Dev* **2007**, *51*, 605−633.
(4) Kim, J. K.; Yang, S. Y.; Lee, Y.; Kim, Y. *Prog. Polym. Sci.* **2010**, *35*, 1325−1349.
(5) Kim, H.-C.; Park, S.-M.; Hinsberg, W. D. *Chem. Rev.* **2010**, *110*, 146−177.
(6) Hardy, C. G.; Tang, C. *J. Polym. Sci., Part B: Polym. Phys.* **2013**, *51*, 2−15.
(7) Gu, X.; Gunkel, I.; Russell, T. P. *Philos. Trans. R. Soc., A* **2013**, *371*, 20120306.
(8) Ross, C. A.; Berggren, K. K.; Cheng, J. Y.; Jung, Y. S.; Chang, J.-B. *Adv. Mater.* **2014**, *26*, 4386−4396.
(9) Wang, J.-Y.; Chen, W.; Russell, T. P. Patterning with Block Copolymers. In *Unconventional Nanopatterning Techniques and Applications*; Rogers, J. A., Lee, H. H., Eds.; John Wiley & Sons: Hoboken, NJ, 2009; pp 233−289.
(10) Segalman, R. A. *Mater. Sci. Eng., R* **2005**, *48*, 191−226.
(11) Darling, S. B. *Prog. Polym. Sci.* **2007**, *32*, 1152−1204.
(12) Bang, J.; Jeong, U.; Ryu, D. Y.; Russell, T. P.; Hawker, C. J. *Adv. Mater.* **2009**, *21*, 4769−4792.

DOI: 10.1021/acs.macromol.5b01028
Macromolecules 2015, 48, 5339−5347

(13) Hamley, I. W. *Prog. Polym. Sci.* **2009**, *34*, 1161−1210.
(14) Marencic, A. P.; Register, R. A. *Annu. Rev. Chem. Biomol. Eng.* **2010**, *1*, 277−297.
(15) Wyman, I.; Liu, G. J. *Sci. China: Chem.* **2013**, *56*, 1040−1066.
(16) Luo, M.; Epps, T. H., III *Macromolecules* **2013**, *46*, 7567−7579.
(17) Hu, H.; Gopinadhan, M.; Osuji, C. O. *Soft Matter* **2014**, *10*, 3867−3889.
(18) Berry, B. C.; Bosse, A. W.; Douglas, J. F.; Jones, R. L.; Karim, A. *Nano Lett.* **2007**, *7*, 2789−2794.
(19) Yager, K. G.; Fredin, N. J.; Zhang, X.; Berry, B. C.; Karim, A.; Jones, R. L. *Soft Matter* **2010**, *6*, 92−99.
(20) Morkved, T. L.; Lu, M.; Urbas, A. M.; Ehrichs, E. E.; Jaeger, H. M.; Mansky, P.; Russell, T. P. *Science* **1996**, *273*, 931−933.
(21) Mansky, P.; DeRouchey, J.; Russell, T. P.; Mays, J.; Pitsikalis, M.; Morkved, T.; Jaeger, H. *Macromolecules* **1998**, *31*, 4399−4401.
(22) Majewski, P. W.; Gopinadhan, M.; Osuji, C. O. *J. Polym. Sci., Part B: Polym. Phys.* **2012**, *50*, 2−8.
(23) Park, S.-M.; Berry, B. C.; Dobisz, E.; Kim, H.-C. *Soft Matter* **2009**, *5*, 957−961.
(24) Park, S.; Lee, D. H.; Xu, J.; Kim, B.; Hong, S. W.; Jeong, U.; Xu, T.; Russell, T. P. *Science* **2009**, *323*, 1030−1033.
(25) De Rosa, C.; Park, C.; Lotz, B.; Wittmann, J.-C.; Fetters, L. J.; Thomas, E. L. *Macromolecules* **2000**, *33*, 4871−4876.
(26) Segalman, R. A.; Yokoyama, H.; Kramer, E. J. *Adv. Mater.* **2001**, *13*, 1152−1155.
(27) Kim, S. O.; Solak, H. H.; Stoykovich, M. P.; Ferrier, N. J.; de Pablo, J. J.; Nealey, P. F. *Nature* **2003**, *424*, 411−414.
(28) Ruiz, R.; Kang, H.; Detcheverry, F. A.; Dobisz, E.; Kercher, D. S.; Albrecht, T. R.; de Pablo, J. J.; Nealey, P. F. *Science* **2008**, *321*, 936−939.
(29) Keller, A.; Pedemonte, E.; Willmouth, F. M. *Nature* **1970**, *225*, 538−539.
(30) Hadziioannou, G.; Picot, C.; Skoukios, A.; Ionescu, M.-L.; Mathis, A.; Duplessix, R.; Gallot, Y.; Lingelser, J.-P. *Macromolecules* **1982**, *15*, 263−267.
(31) Morrison, F. A.; Winter, H. H. *Macromolecules* **1989**, *22*, 3533−3540.
(32) Morrison, F. A.; Winter, H. H.; Gronski, W.; Barnes, J. D. *Macromolecules* **1990**, *23*, 4200−4205.
(33) Morrison, F. A.; Mays, J. W.; Muthukumar, M.; Nakatani, A. I.; Han, C. C. *Macromolecules* **1993**, *26*, 5271−5273.
(34) Angelescu, D. E.; Waller, J. H.; Adamson, D. H.; Deshpande, P.; Chou, S. Y.; Register, R. A.; Chaikin, P. M. *Adv. Mater.* **2004**, *16*, 1736−1740.
(35) Pelletier, V.; Asakawa, K.; Wu, M.; Adamson, D. H.; Register, R. A.; Chaikin, P. M. *Appl. Phys. Lett.* **2006**, *88*, 211114.
(36) Papalia, J. M.; Adamson, D. H.; Chaikin, P. M.; Register, R. A. *J. Appl. Phys.* **2010**, *107*, 084305.
(37) Kim, S. Y.; Gwyther, J.; Manners, I.; Chaikin, P. M.; Register, R. A. *Adv. Mater.* **2014**, *26*, 791−795.
(38) Kwon, H.-K.; Lopez, V. E.; Davis, R. L.; Kim, S. Y.; Burns, A. B.; Register, R. A. *Polymer* **2014**, *55*, 2059−2067.
(39) Davis, R. L.; Chaikin, P. M.; Register, R. A. *Macromolecules* **2014**, *47*, 5277−5285.
(40) Garcia, N. A.; Davis, R. L.; Kim, S. Y.; Chaikin, P. M.; Register, R. A.; Vega, D. A. *RSC Adv.* **2014**, *4*, 38412−38417.
(41) Kim, S. Y.; Nunns, A.; Gwyther, J.; Davis, R. L.; Manners, I.; Chaikin, P. M.; Register, R. A. *Nano Lett.* **2014**, *14*, 5698−5705.
(42) Angelescu, D. E.; Waller, J. H.; Register, R. A.; Chaikin, P. M. *Adv. Mater.* **2005**, *17*, 1878−1881.
(43) Pujari, S.; Keaton, M. A.; Chaikin, P. M.; Register, R. A. *Soft Matter* **2012**, *8*, 5358−5363.
(44) Singh, G.; Yager, K. G.; Berry, B.; Kim, H.-C.; Karim, A. *ACS Nano* **2012**, *6*, 10335−10342.
(45) Majewski, P. W.; Yager, K. G. *ACS Nano* **2015**, *9*, 3896−3906.
(46) Ye, C.; Singh, G.; Wadley, M. L.; Karim, A.; Cavicchi, K. A.; Vogt, B. D. *Macromolecules* **2013**, *46*, 8608−8615.
(47) Jeong, J. W.; Hur, Y. H.; Kim, H.-J.; Kim, J. M.; Park, W. I.; Kim, M. J.; Kim, B. J.; Jung, Y. S. *ACS Nano* **2013**, *7*, 6747−6757.
(48) Qiang, Z.; Zhang, Y.; Groff, J. A.; Cavicchi, K. A.; Vogt, B. D. *Soft Matter* **2014**, *10*, 6068−6076.
(49) Qiang, Z.; Zhang, L.; Stein, G. E.; Cavicchi, K. A.; Vogt, B. D. *Macromolecules* **2014**, *47*, 1109−1116.
(50) Wu, M. W.; Register, R. A.; Chaikin, P. M. *Phys. Rev. E* **2006**, *74*, 040801.
(51) Marencic, A. P.; Wu, M. W.; Register, R. A.; Chaikin, P. M. *Macromolecules* **2007**, *40*, 7299−7305.
(52) Marencic, A. P.; Adamson, D. H.; Chaikin, P. M.; Register, R. A. *Phys. Rev. E* **2010**, *81*, 011503.
(53) Marencic, A. P.; Chaikin, P. M.; Register, R. A. *Phys. Rev. E* **2012**, *86*, 021507.
(54) Pelletier, V.; Adamson, D. H.; Register, R. A.; Chaikin, P. M. *Appl. Phys. Lett.* **2007**, *90*, 163105.
(55) Nikoubashman, A.; Davis, R. L.; Michal, B. T.; Chaikin, P. M.; Register, R. A.; Panagiotopoulos, A. Z. *ACS Nano* **2014**, *8*, 8015−8026.
(56) Bushuk, W.; Benoît, H. *Can. J. Chem.* **1958**, *36*, 1616−1626.
(57) Register, R. A.; Bell, T. R. *J. Polym. Sci., Part B: Polym. Phys.* **1992**, *30*, 569−575.
(58) Ferry, J. D. *Viscoelastic Properties of Polymers*, 3rd ed.; Wiley: New York, 1980; p 277.
(59) Morrison, F. A. *Understanding Rheology*; Oxford University Press: New York, 2001; pp 397−401.
(60) Bird, R. B.; Armstrong, R. C.; Hassager, O. *Dynamics of Polymeric Liquids*, 2nd ed.; Wiley: New York, 1987; Vol *1*.
(61) Hamley, I. W. *Macromol. Theory Simul.* **2000**, *9*, 363−380.
(62) Chaikin, P. M.; Lubensky, T. C. *Principles of Condensed Matter Physics*; Cambridge University Press: New York, 1995; pp 144−212.
(63) Ruzette, A.-V. G.; Banerjee, P.; Mayes, A. M.; Pollard, M.; Russell, T. P.; Jerome, R.; Slawecki, T.; Hjelm, R.; Thiyagarajan, P. *Macromolecules* **1998**, *31*, 8509−8516.
(64) Ahn, H.; Naidu, S.; Ryu, D. Y.; Cho, J. *Macromol. Rapid Commun.* **2009**, *30*, 469−474.
(65) Efron, B.; Tibshirani, R. *Stat. Sci.* **1986**, *1*, 54−75.
(66) Bartels, C. R.; Crist, B.; Graessley, W. W. *Macromolecules* **1984**, *17*, 2702−2708.
(67) Lodge, T. P. *Phys. Rev. Lett.* **1999**, *83*, 3218−3221.
(68) Rubinstein, M.; Colby, R. H. *Polymer Physics*; Oxford University Press: New York, 2003.
(69) Lodge, T. P.; Dalvi, M. C. *Phys. Rev. Lett.* **1995**, *75*, 657−660.
(70) Yokoyama, H.; Kramer, E. J. *Macromolecules* **1998**, *31*, 7871−7876.
(71) Yokoyama, H.; Kramer, E. J.; Fredrickson, G. H. *Macromolecules* **2000**, *33*, 2249−2257.
(72) Harrison, C.; Park, M.; Chaikin, P. M.; Register, R. A.; Adamson, D. H.; Yao, N. *Polymer* **1998**, *30*, 2733−2744.
(73) Harrison, C.; Chaikin, P. M.; Huse, D. A.; Register, R. A.; Adamson, D. H.; Daniel, A.; Huang, E.; Mansky, P.; Russell, T. P.; Hawker, C. J.; Egolf, D. A.; Melnikov, I. V.; Bodenschatz, E. *Macromolecules* **2000**, *33*, 857−865.

DOI: 10.1021/acs.macromol.5b01028
Macromolecules 2015, 48, 5339−5347